J|A|C|S ARTICLES

Published on Web 11/10/2009

Dots versus Antidots: Computational Exploration of Structure, Magnetism, and Half-Metallicity in Boron−Nitride Nanostructures

Aijun Du,[†] Ying Chen,[‡] Zhonghua Zhu,[§] Rose Amal,[||] Gao Qing (Max) Lu,[⊥] and Sean C. Smith*,[†]

Australian Institute for Bioengineering and Nanotechnology, Centre for Computational Molecular Science, The University of Queensland, QLD 4072, Brisbane, Australia, Institute for Technology Research and Innovation, Deakin University, Waurn Ponds, Victoria 3217, Australia, School of Chemical Engineering, The University of Queensland, QLD 4072, Brisbane, Australia, ARC Centre of Excellence for Functional Nanomaterials, School of Chemical Sciences and Engineering, University of New South Wales, Sydney, NSW 2052, Australia, and Australian Institute for Bioengineering and Nanotechnology, ARC Centre of Excellence for Functional Nanomaterials, The University of Queensland, QLD 4072, Brisbane, Australia

Received August 25, 2009; E-mail: s.smith@uq.edu.au

Abstract: Triangle-shaped nanohole, nanodot, and lattice antidot structures in hexagonal boron−nitride (h-BN) monolayer sheets are characterized with density functional theory calculations utilizing the local spin density approximation. We find that such structures may exhibit very large magnetic moments and associated spin splitting. N-terminated nanodots and antidots show strong spin anisotropy around the Fermi level, that is, half-metallicity. While B-terminated nanodots are shown to lack magnetism due to edge reconstruction, B-terminated nanoholes can retain magnetic character due to the enhanced structural stability of the surrounding two-dimensional matrix. In spite of significant lattice contraction due to the presence of multiple holes, antidot super lattices are predicted to be stable, exhibiting amplified magnetism as well as greatly enhanced half-metallicity. Collectively, the results indicate new opportunities for designing h-BN-based nanoscale devices with potential applications in the areas of spintronics, light emission, and photocatalysis.

Introduction

Low-dimensional materials, such as single-layered graphite, or graphene have been the subject of intensive research[1−4] in the past five years due to considerable promise for the fabrication of nanoscale devices.[5−7] Hexagonal boron−nitride (h-BN) has a similar structure to graphene but in contrast displays insulator characteristics.[8] Experimentally, single layer graphene-like h-BN nanosheets have been produced on a SiO_2 substrate in the Zettl group.[9] Recently, Jin et al. and Meyer et al. have respectively fabricated free-standing h-BN single layers by controlled energetic electron beam irradiation through a sputter process.[10,11] Atomic defects in h-BN have been characterized and compared to those observed in graphene membranes.[11,12] However, novel magnetic properties have not as yet been addressed. Theoretically, several studies have revealed that the edge structure of h-BN nanoribbons plays an important role on the electronic and magnetic properties.[13−15] Recently, the UQ lab has systematically investigated atomic and electronic structure in zigzag and armchair BN nanoribbons.[16] Defects in an h-BN monolayer have been studied by Azevedo et al.;[17,18] however, the formation energy for a single B vacancy defect (V_B) was predicted to be higher than that of a single N vacancy defect (V_N), which

[†] Centre for Computational Molecular Science, The University of Queensland.
[‡] Deakin University.
[§] School of Chemical Engineering, The University of Queensland.
[||] University of New South Wales.
[⊥] ARC Centre of Excellence for Functional Nanomaterials, The University of Queensland.

(1) Novoselov, K. S.; Geim, A. K.; Morozov, S. V.; Jiang, D.; Zhang, Y.; Dubonos, S. V.; Grigorieva, I. V.; Firsob, A. A *Science* **2004**, *306*, 666.
(2) Geim, A. K.; Novoselov, K. S. *Nat. Mater.* **2007**, *6*, 183.
(3) Berger, C.; Song, Z. M.; Li, X. B.; Wu, X. S.; Brown, n.; Naud, C.; Mayo, D.; Li, T. B.; Hass, J.; Marchenkov, A. n.; Conrad, E. H.; First, P. n.; de Heer, W. A. *Science* **2006**, *312*, 1191.
(4) Novoselov, K. S.; Geim, A. K.; Morozov, S. V.; Jiang, D.; Katsnelson, M. I.; Grigorieva, I. V.; Dubonos, S. V.; Firsov, A. A. *Nature (London)* **2005**, *438*, 197.
(5) Falko, V. *Nat. Phys.* **2007**, *3*, 151.
(6) Son, Y. W.; Cohen, M. L.; Louie, S. G. *Nature* **2006**, *444*, 347.
(7) Wang, X. R.; Li, X. L.; Zhang, L.; Yoon, Y.; Weber, P. K.; Wang, H. L.; Guo, J.; Dai, H. J. *Science* **2009**, *324*, 5928.
(8) Novoselov, K. S.; Jiang, D.; Schedin, F.; Booth, T.; Khot-kevich, V. V.; Morozov, S.; Geim, A. K. *Proc. Natl. Acad. Sci. U.S.A.* **2005**, *102*, 10451.
(9) Pacile, D.; Meyer, J. C.; Girit, C. O.; Zettl, A. *Appl. Phys. Lett.* **2008**, *92*, 133107.
(10) Jin, C. H.; Lin, F.; Suenaga, K.; Iijima, S. *Phys. Rev. Lett.* **2009**, *102*, 195505.
(11) Meyer, J. C.; Chuvilin, A.; Algara-Siller, G.; Biskupek, J.; Kaiser, U. *Nano Lett.* **2009**, *9*, 2683.
(12) Zobelli, A.; Ewels, C. P.; Gloter, A.; Seifert, G. *Phys. Rev. B* **2007**, *75*, 094104.
(13) Park, C. H.; Louie, S. G. *Nano Lett.* **2008**, *8*, 2200.
(14) Barone, V.; Peralta, J. E. *Nano Lett.* **2008**, *8*, 2210.
(15) Zhang, Z. H.; Guo, W. L. *Phys. Rev. B* **2008**, *77*, 075403.
(16) Du, A. J.; Lu, G. Q.; Smith, S. C. *Chem. Phys. Lett.* **2007**, *447*, 181.
(17) Azevedo, S.; Kaschny, J. R.; de Castilho, C. M. C.; de Brito Mota, F. *Nanotechnology* **2007**, *18*, 495707.
(18) Azevedo, S.; Kaschny, J. R.; de Castilho, C. M. C.; de Brito Mota, F. *Eur. Phys. J. B* **2009**, *67*, 507.

 10.1021/ja9071942 CCC: $40.75

contrasts with recent experimental findings.[10,11] Bare N atoms at zigzag edges in open-ended BN nanotubes and AlN/BN nanoribbons were also found to display an enormous spin-splitting[19−21] and strong spin transport anisotropy, respectively. These findings offer much potential for the development of new devices and applications in spintronics.

The present study is prompted by the observation that edges in triangle-shaped nanoholes and nanodots are all zigzag-like with regard to B/N termination and as such may be anticipated to carry large magnetic moments similar to graphene[22] and possess strong spin-polarization at the Fermi level as in the case of BN/AlN nanoribbons.[20,21] We have performed *ab initio* density functional theory calculations based on the local spin density approximation designed to systematically explore this class of triangular nanohole, nanodot or antidot superlattices in an h-BN monolayer. In contrast to previous studies, we find that a V_B monovacancy has the lower formation energy in comparison with the V_N monovacancy in an N-rich environment, which may clarify the preferred orientation (i.e., that corresponding to V_B) of such triangular defects observed in recent experiments. Triangular nanoholes, nanodots and antidots created from an h-BN monolayer are found to carry remarkably large magnetic moments and exhibit strong spin transport anisotropy around the Fermi level due to N/B atoms with open shell character at the zigzag edges. These results suggest new avenues toward spintronics and enhanced photo catalysis applications through the sculpting of graphene-like h-BN fragments. In the next section, we summarize the computational method. Section III presents the structural, novel magnetic and electronic properties for nanohole, nanodot and antidot lattice structures in an h-BN monolayer. The last section is devoted to conclusions.

Computational Details

All calculations were performed by using the plane-wave basis VASP code[23,24] implementing the local spin density approximation (LSDA) exchange correlation functional[25] since previous studies have shown that LSDA is more reliable for h-BN systems.[26] An all-electron description, the projector augmented wave method (PAW)[27,28] is used to describe the electronic-ion-core interaction. The lattice constant for a h-BN monolayer was calculated to be 2.49 Å, which is in good agreement with the experimental value.[29] A 10 × 10 h-BN monolayer containing 200 atoms ($24.9 \times 24.9 \times 18$ Å^3) is used for exploring nanoholes in an h-BN monolayer. B or N terminated triangle nanodots were studied by using a cubic supercell ($30 \times 30 \times 15$ Å^3) with a vacuum space of 15 Å in X, Y and Z dimensions, which is enough to separate the defect interaction between periodic images. The cutoff energies for plane waves are chosen to be 500 eV and only the Γ point is used for sampling the Brillium zone due to the large supercell used. All the atoms in the supercell were allowed to relax and the force tolerance was set at 0.005 eV/Å.

Results and Discussion

As a preliminary point of comparison with earlier work,[17,18] we characterized the properties of atomic defects in h-BN. Single nitrogen (V_N) and boron (V_B) vacancies were created by removing single N or B atoms from an h-BN monolayer. Geometries were subsequently optimized with the conjugated gradient method and the formation energy was calculated as has been described previously[17] (for more details see the Supporting Information). Previous theoretical studies indicated that the V_N defect is the preferred defect in an h-BN monolayer,[17,18] in contrast with recent experimental findings.[9,10] Our calculated formation energies indicate, however, that V_N is only more stable than V_B in a B-rich environment. Contrastingly, in an N-rich environment (e.g., atmospheric) we calculate the V_B formation energy to be 7.62 eV. This is 0.62 eV lower than that calculated for V_N (8.24 eV), indicating that the V_B defect is preferred in an h-BN monolayer. Possible reasons for our different result in comparison with the earlier theoretical study[17,18] could be that a more generous force tolerance (0.06 eV/Å) and smaller unit cell were used in the previous work, leading to a less completely relaxed configuration. For example ref.[16] reported 3 μB for V_B defect, but we found the magnetic moment will reduce to 1 μB during optimization. Our results (in N-rich environment) are in good agreement with the finding that only V_B defect is experimentally detected. In Figure 1a and 1b, we present the optimized geometries for V_B and V_N, respectively. The orientations of the triangular V_B and V_N defects are mutually inverted, that is, the B-edged V_N vacancy points downward while the N-edged (V_B) vacancy points upward with the supercell as drawn in Figure 1. The N−N distances for the three adjacent neighbors are 2.57, 2.57, and 2.71 Å (asymmetric), greater than the corresponding distance (2.49 Å) in a perfect h-BN monolayer. In contrast the B−B distances for the three adjacent neighbors are all 2.26 Å (Symmetric), less than the corresponding distance (also 2.49 Å) in the perfect h-BN monolayer. Both V_B and V_N monovacancies are found to be ferromagnetic with 1 μB magnetic moment due to unpaired electron density at the edge N/B atoms. The net spin density of the occupied levels is also apparent from inspection of the spin-resolved density of states as shown in Figure 1c and d, respectively. The magnetic charge densities are mainly localized around edge N (major contribution from P_x and P_y orbitals) and B (major contribution from Pz orbital) atoms for V_B and V_N, respectively (see Figure S1 and S2 in the Supporting Information).

Larger defects (multivacancies) in an h-BN monolayer are of considerable interest due to the potential for enhanced magnetic moment and spin filtering properties. We explore this by carrying out calculations for the following scenarios: (i) removing one B and three N atoms (V_{B+3N}), (ii) removing one N and three B atoms (V_{N+3B}), (iii) removing three B and six N atoms (V_{3B+6N}), and (iv) removing three N and six B atoms (V_{3N+6B}), respectively. All of these defect structures yield triangle shaped nanoholes prior to optimization, with either N or B termination along the zigzag edges. Figure 2 presents the optimized geometries for each of these defect arrangements. The V_{N+3B} and V_{B+3N} triangular nanoholes are apparently strongly reconstructed. The B−B and N−N distances for the six first-neighbors are 1.96 and 1.60 Å (very close to single

(19) Hao, S. G.; Zhou, G.; Duan, W. H.; Wu, J.; Gu, B. L. *J. Am. Chem. Soc.* **2006**, *128*, 8453.
(20) Zheng, F. W.; Zhou, G.; Liu, Z. R.; Wu, J.; Duan, W. H.; Gu, B. L.; Zhang, S. B. *Phys. Rev. B* **2008**, *78*, 205415.
(21) Du, A. J.; Zhu, Z. H.; Chen, Y.; Lu, G. Q.; Smith, S. C. *Chem. Phys. Lett.* **2009**, *469*, 183.
(22) Wang, W. L.; Meng, S.; Kaxiras, E. *Nano Lett.* **2008**, *8*, 241.
(23) Kresse, G.; Furthmuller, J. *Comput. Mater. Sci.* **1996**, *6*, 15.
(24) Kresse, G.; Furthmuller, J. *Phys. Rev. B* **1996**, *54*, 11169.
(25) Ceperley, D. M.; Alder, B. J. *Phys. Rev. Lett.* **1980**, *45*, 566.
(26) Kern, G.; Kresse, G.; Hafner, J. *Phys. Rev. B* **1999**, *59*, 8551.
(27) Blochl, P. E. *Phys. Rev. B* **1994**, *50*, 17953.
(28) Kresse, G.; Joubert, D. *Phys. Rev. B* **1999**, *59*, 1758.
(29) Nagashima, A.; Tejima, N.; Gamou, Y.; Kawai, T.; Oshima, C. *Phys. Rev. Lett.* **1995**, *75*, 3918.

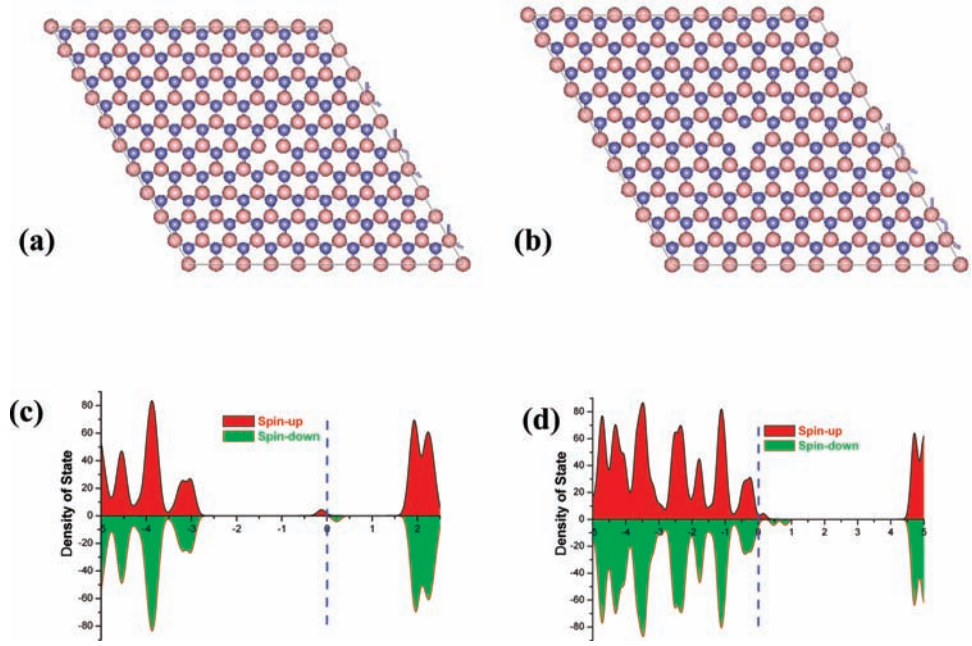

Figure 1. (a) Optimized geometry for a vacancy created by removal of a N atom from a hexagonal 10 × 10 BN nanosheet (N monovacancy). Pink and blue balls represent B and N atoms, respectively. (b) Same as for (a) but where a B atom is removed instead. (c) Spin-resolved density of states associated with the system depicted in (a). (d) Spin-resolved density of states associated with (b).

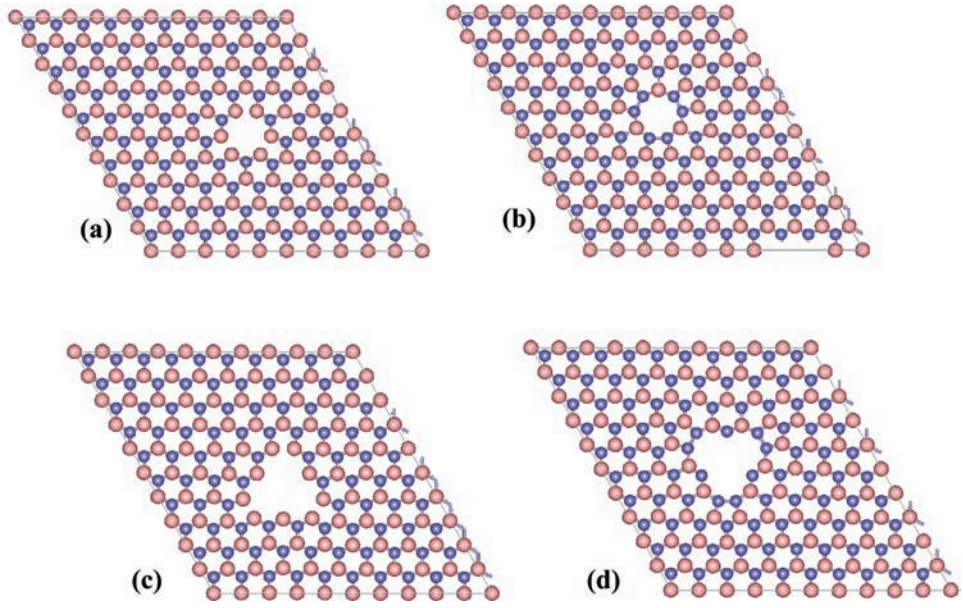

Figure 2. (a) Optimized geometry for an h-BN sheet incorporating a B-terminated nanohole (V_{B+3N}). (b) Same as (a) but for an N-terminated nanohole (V_{N+3B}). (c) Same as (a) but for a V_{3B+6N} defect. (d) Same as (a) but for V_{3N+6B} defect. Pink and blue balls represent B and N atoms, respectively.

B−B and N−N bond length) for V_{B+3N} and V_{N+3B}, respectively. Obviously, chemical bonds are formed between B−B (N−N) atoms, leading to nonmagnetic system due to the spin pairing associated with these bonds. For the larger V_{3N+6B} and V_{3B+6N} defects, we found that only neighboring B (N) atoms around the corners of the holes will bind with each other, leaving the other three B or N atoms in the middle of each edge with unpaired electrons. Both V_{3N+6B} and V_{3B+6N} multivacancies hence possess a magnetic moment of 3 μB. Still larger triangular vacancy defects are not explored in isolation here due to the fact that a very large supercell has to be used to avoid the defect interaction between periodic images and this exceeds the current limitations of our computational resources. One can, however, consider larger nanoholes in the context of a patterned array, which then implicitly includes the defect−defect coupling (Figure 4 below). On the basis of the results here, it may be anticipated that larger vacancy defects (i.e., with more than 9 B/N edge terminating atoms) should display substantial magnetism and spin-splitting—roughly in proportion to the number of unpaired electrons of the N/B atoms along the zigzag edges.

Nanodots are the structural complement to the vacancy defects explored above for an h-BN monolayer. Hence, it is informative to examine also the electronic and structural properties of B/N terminated triangular nanodots. Figure 3 presents the optimized geometries for three representative BN triangular nanodots. It is apparent that the B-terminated nanodot (Figure 3a) becomes

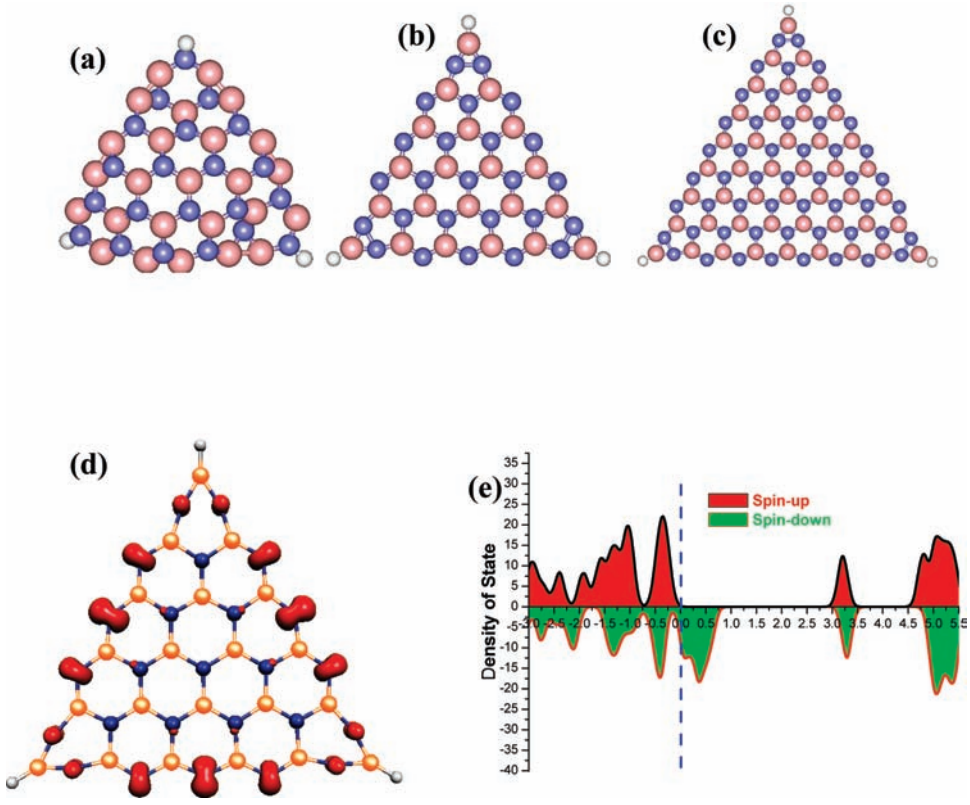

Figure 3. (a) Optimized geometry for a B-terminated BN triangular nanodot. (b) Optimized geometry for an N-terminated BN triangular nanodot. (c) Same as for (b) but with a larger system containing 100 atoms. (d) Three dimensional spin magnetic charge density ($\rho_\uparrow - \rho_\downarrow$) corresponding to the system in (b). (e) Spin-resolved density of states plot corresponding to the system in (b). Pink and blue balls represent B and N atoms, respectively.

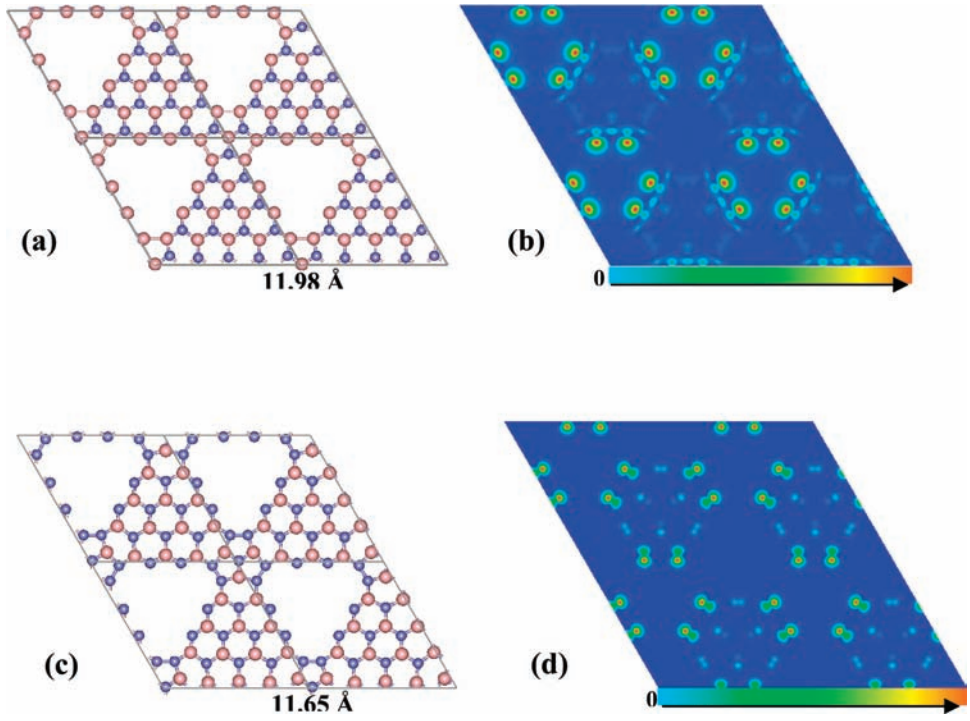

Figure 4. (a) and (c) Optimized geometries of triangular antidot BN super lattices with B and N termination respectively. (b) and (d) Planar projection of the magnetic charge density ($\rho_\uparrow - \rho_\downarrow$) for (a) and (b), respectively.

strongly distorted with substantial B−B bond formation around the edges. This bond formation has the effect of spin pairing most of the "spare" valence electrons of the B edge atoms, such that the B-terminated nanodot is nonmagnetic in its ground state. This structural effect is entirely analogous to that demonstrated previously for BN nanotubes[19] as well as BN nanoribbons.[20] The contrast between the nonmagnetic ground state for the B-terminated nanodot of Figure 3a (15 B edge atoms) and the

magnetism of the smaller B-terminated nanohole of Figure 2c (just 9 B edge atoms) highlights the significant structural role of the two-dimensional lattice in largely stabilizing the B-terminated nanoholes. The N-terminated nanodots (Figure 3b and c) display a greater degree of stability with respect to stabilizing edge N atoms with unpaired electrons: only the corner N atoms are seen to reconstruct and the system is predicted to possess a very large magnetic moment (9 and 18 μB for Figures 3b and 3c, respectively). The added stability of the N-terminated edges can be simply rationalized by the fact that the N atoms possess 2 additional electrons that participate in the π-bonding network. Again, this is entirely consistent with the previous demonstration of magnetic properties of bare N-terminated edges in BN nanoribbons and also AlN nanoribbons.[20,21] Figure 3d presents a three-dimensional spin magnetic charge density ($\rho_\uparrow - \rho_\downarrow$) plot (iso-value is 0.18 e/Å^3) for the N-terminated nanodot of Figure 3b. Clearly, the large net magnetism is attributable primarily to the N-atom dangling bonds at the zigzag edges. Most interestingly, the N-terminated BN nanodot also displays a complete spin-polarization around the Fermi level as shown clearly in the spin-resolved density of states plot in Figure 3e. In light of the magnetic charge density plot of Figure 3d, this intrinsic spin transport anisotropy, that is, half-metallicity, appears predominantly due to the open shell dangling bonds (P_x and P_y orbitals of edge N atoms as shown in Figure S3 in the Supporting Information) on the bare nitrogen atoms at the zigzag edges. We have further tested the stability of the N-terminated BN nanodot by implementing finite temperature ($T = 573$ K) ab initio molecular dynamics (AIMD) simulations using a time step of 0.5 fs. The N-terminated triangle nanodot of Figure 3b is observed in the AIMD simulations to be stable up to 2 ps.

Graphene antidot superlattices have been found to display intriguing electronic properties around the Fermi level as recently reported by Pedersen et al. and Park et al., respectively.[30,31] To conclude this discussion, we explore the properties of an h-BN monolayer with regularly spaced triangular holes. This type of antidot superlattice structure could be very interesting for building low dimensional BN-based electronic circuits, since open shell N/B atoms at zigzag edges possess large spin-splitting as alluded to above. Geometry optimizations were first performed with variation of the lattice parameter. Large lattice compressions of 3.8% and 5.5% were respectively found for the B and N-terminated antidot super lattices. Figure 4a and c presents the optimized geometries, from which it is apparent that corner B/N atoms are reconstructed by forming B−B/N−N bonds. The other B/N edge atoms retain open shell character and collectively exhibit large magnetism as shown in Figure 4b and d, which shows the projection of magnetic charge density ($\rho_\uparrow$-$\rho_\downarrow$) in the XOY plane. In Figure 5, we present plots of the spin-resolved density of states (DOS) for (a) a pure h-BN monolayer, (b) the B-terminated antidote super lattice (Figure 4a), and (c) the N-terminated antidots super lattice (Figure 4c). As expected, the pure h-BN monolayer is a large gap (4.6 eV) insulator. With the introduction of B/N terminated nanoholes, the gap is reduced greatly and the systems show large net magnetic moments due to the open shell N/B edge atoms. Similar to the N-terminated nanodot (Figure 3e), the N-terminated antidot super lattice displays complete spin-polarization around the Fermi level, suggesting potential application in spintronics. One potentially significant advantage of a two-dimensional patterned array of such antidots, burned or etched in the supporting BN monolayer, is that the requisite spatial alignment of spin filtering components would automatically be incorporated by the lattice. This physical alignment presumably would be more difficult to achieve when individual molecules, ribbons, or nanotubes are to be utilized for the spin filtering.

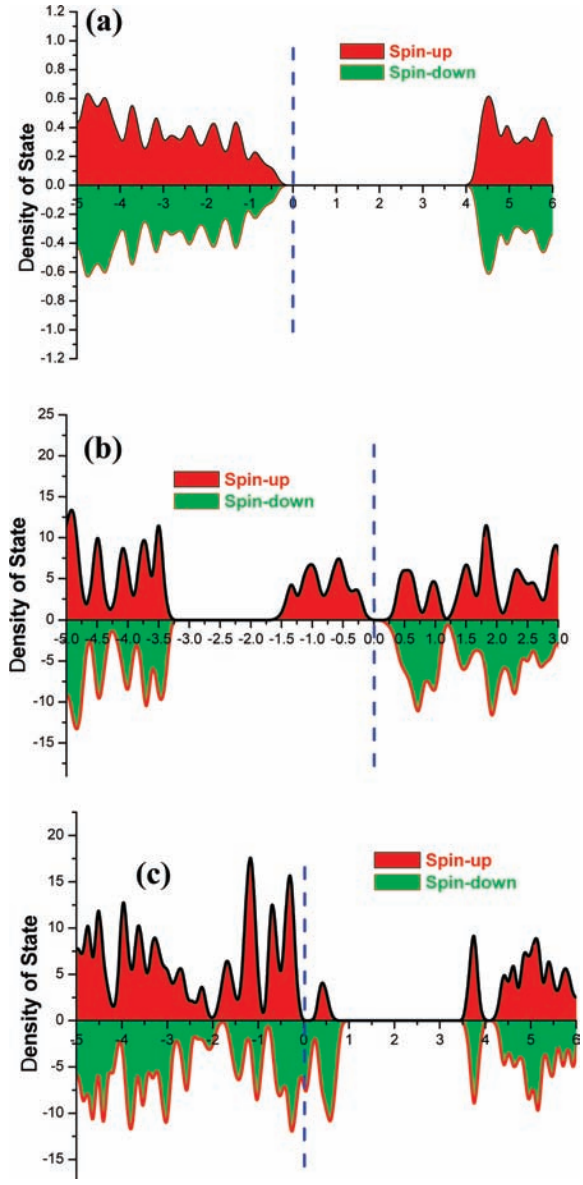

Figure 5. Spin-resolved total density of states corresponding to (a) a perfect 10 × 10 h-BN monolayer; (b) B-terminated antidot super lattice of Figure 4a; and (c) the N-terminated antidot super lattice of Figure 4c.

It is also possible that optical properties may potentially be tuned in B/N terminated nanodots and antidots to enable, e.g., visible light emission or absorption. It can be seen clearly from the plots of spin-resolved densities of states (see Figures 3e and 5b and c) that the open shell B and N edge atoms have substantial effects on the conduction band, the valence band and the band gap structure. Additional flexibility may be provided by exploring the effects of differently shaped nanoholes. It is worthy of note that experiments have recently been reported demonstrating that graphitic carbon nitride (g-C_3N_4) is a promising candidate for producing hydrogen from water

(30) Pedersen, T. G.; Flindt, C.; Pedersen, J.; Mortesen, N. A.; Jauho, A. P.; Pedersen, K. *Phys. Rev. Lett.* **2008**, *100*, 136804.
(31) Park, C. H.; Yang, L.; Son, Y. W.; Cohen, M. L.; Louie, S. G. *Nat. Phys.* **2008**, *4*, 213.

under visible light.[32] In those studies the bare edge N atoms were found to be responsible for visible light absorption. The patterning of an h-BN monolayer with an array of vacancy defects containing similarly reactive open shell N edge atoms may therefore provide a simple and powerful alternative route to splitting water for hydrogen production under visible light. In practice, the synthesis of BN nanodot or antidot superlattice structures is experimentally achievable through sculpting h-BN fragments with the development of novel etching, e-beam lithography or patterned ion-beam implantation technology. Near-edge X-ray absorption final structure (NEXAFS) measurement can detect effectively dots and antidots from h-BN crystals.[33]

Conclusions

Graphene-like boron nitride nanohole, nanodot and antidot superlattice structures have been investigated by *ab initio* density functional theory calculations. Many of these structures are found to carry large magnetic moments and spin-splitting. Most interestingly, N-terminated nanodots and antidots are found to be stable well above room temperature and exhibit near-complete intrinsic spin-polarization at the Fermi level, leading to spin transport anisotropy. Additionally, HOMO−LUMO gaps in both nanodots and antidots are found to be greatly reduced in comparison with that of a pristine h-BN monolayer, suggesting the possibility of tunable light absorption/emission at visible wavelengths. Collectively, the results of this work offer many possibilities for future development of spintronics, light emission and enhanced photo catalysis applications by the sculpting of graphene-like h-BN fragments.

Acknowledgment. We acknowledge generous grants of high-performance computer time from both the Computational Molecular Science cluster computing facility at The University of Queensland and the Australian Partnership for Advanced Computing (APAC) National Facility. The authors also greatly appreciate the financial support of the Australian Research Council and The University of Queensland through the ARC Centre of Excellence for Functional Nanomaterials.

Supporting Information Available: More details on computing the formation energy of B or N monovacancy, magnetic charge density for V_B and V_N (Figure S1), site (B or N atoms) and p-orbital resolved project density of state for V_B and V_N (Figure S2), project density of state on B and N atoms (Figure 3e) for N-terminated triangle nanodot (Figure S3), project density of state (Figure S4) on B and N atoms and a 3D isosurface magnetic charge density plot (Figure S5) for B or N terminated antidot superlattice. This material is available free of charge via the Internet at http://pubs.acs.org.

JA9071942

(32) Wang, X. C.; Maeda, K.; Thomas, A.; Takanabe, K.; Xin, G.; Carlsson, J. M.; Domen, K.; Antonietti, M. *Nat. Mater.* **2008**, *8*, 76.
(33) Bozanic, A.; Petravic, M.; Fan, L. J.; Wang, Y. W.; Chen, Y. *Chem. Phys. Lett.* **2009**, *472*, 130.